Journal of Statistical Physics, Vol. 81, Nos. 1/2, 1995

Lattice Gas with "Interaction Potential"

Olivier Tribel[1] and Jean Pierre Boon[1]

Received October 6, 1994; final January 10, 1995

We present an extension of a simple automaton model to incorporate nonlocal interactions extending over a spatial range in lattice gases. From the viewpoint of statistical mechanics, the lattice gas with interaction range may serve as a prototype for non-ideal-gas behavior. From the density fluctuations correlation function, we obtain a quantity which is identified as a potential of mean force. Equilibrium and transport properties are computed theoretically and by numerical simulations to establish the validity of the model at macroscopic scale.

KEY WORDS: Lattice gas automata; interaction potential; fluctuation correlation function; spinodal decomposition.

1. LATTICE GAS WITH NONLOCAL INTERACTIONS

Standard lattice gas automata (LGA) evolve according to an iterated sequence of mass- and momentum-preserved local collisions followed by propagation. Nonlocal interactions can be incorporated in the LGA dynamics via long-distance momentum transfer simulating attraction and/or repulsion between particles.[1-3] In local collisions, momentum redistribution is a node-located process with local conservation of mass and momentum. In nonlocal interactions (NLI), momentum is exchanged between two particles residing on nodes separated by a (fixed or variable) distance r: mass is conserved locally, momentum is conserved globally. At the macroscopic level, the main feature exhibited by LGA models with NLIs is a "liquid-gas"-type phase separation with bubble and drop formation.[1] From the statistical mechanical viewpoint, LGAs with NLIs form

[1] Center for Nonlinear Phenomena and Complex Systems, Université Libre de Bruxelles, B-1050 Brussels, Belgium. E-mail: otribel@ulb.ac.be; jpboon@ulb.ac.be.

0022-4715/95/1000-0361$07.50/0

an interesting class of models in that—in contrast to standard collision-propagation models—they include an elementary process which is essential for "nonideal" behavior.

The dynamics of LGA virtual particles is not governed by Newton's equation of motion and the concepts of force and potential cannot be used in the sense of classical mechanics. Moreover, in real fluids each particle is subjected *a priori* to the force field of *all* particles (whose effect is quantified by the potential of mean force), whereas in discrete lattice gases each particle interacts nonlocally with at most *one* other particle at a time. So *stricto sensu* the usual concept of intermolecular potential does not apply to lattice gases.

In the LGA model with NLI's proposed by Tribel and Boon[3] the idea of an interaction range was introduced by governing the interaction distance according to a probability distribution—namely a power law ($\propto r^{-\mu}$)—wherefrom a distance r is drawn for each particle at every time step. Here we show that for sufficiently long times and large number of particles, the implementation of a probability distribution of interaction distance has a resulting effect similar to the effect of an interaction potential. We first describe the model in Section 2. Then in Section 3 we compute the density fluctuation correlations[2] wherefrom a quantity is obtained which can be identified as a potential of mean force. Sections 4 and 5 present an analysis of the equilibrium and transport properties. We conclude with some comments.

2. INTERACTION RANGE MODEL

The automaton resides on a two-dimensional triangular lattice and uses for propagation and local collisions the rules of the FHP-III model[4] with periodic boundary conditions. Nonlocal interactions can take place between two particles when nodes separated by some distance r exhibit favorable configurations as illustrated in Fig. 1. The interaction modifies the orientation of the velocity vectors from a diverging configuration to a converging configuration to simulate attractive forces and *vice versa* for repulsive forces. At each time step, the algorithmic procedure must realize a pairing of particles separated by a distance r drawn from a probability distribution $p(r)$. It is clear that a parallel algorithm can hardly be efficient here. Therefore we use a sequential algorithm which proceeds as follows:

[2] Here we are interested in correlations at distance of the order of the interaction range; long-range and long-time correlations are discussed, respectively in refs. 9 and 10.

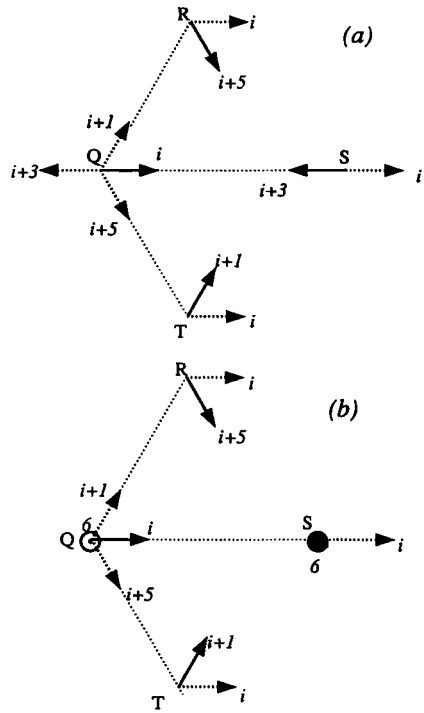

Fig. 1. Interaction configurations: configuration changes through nonlocal interactions between pairs of particles on nodes at distance r from each other. Dotted (full) arrows indicate channel occupation before (after) interaction: $[Q_j, X_k] \rightarrow [Q_k, X_j]$, $X = R, S, T$, where the channel indices (j, k) are given modulo 6 for $i = 0,..., 5$. Momentum exchange through interactions is two or four units for (a) configurations, whereas all (b) interactions exchange two momentum units.

(i) At each time step, a direction is arbitrarily chosen along any of the lattice axes and all interactions will be along that direction during that time step.

(ii) A particle, say at node A, is (sequentially) selected and accepted if its state has not been modified by a previous interaction in the sequential procedure.

(iii) A distance r is drawn from the distribution $p(r)$ and a pointer is set at nodes F and B, located, respectively, at a distance r forward and backward from A.

(iv) If one of the configurations "BA" or "AF" is compatible for interaction (see Fig. 1), the configuration is modified accordingly

and the procedure keeps track of the modification for the duration of the sequence (each particle can undergo no more than one interaction per time step).

As a result, the effective probability that an interaction occurs in the simulation differs from the theoretical $p(r)$. The details of the computation are given in the appendix; here we merely quote the final result, which expresses the *effective probability* $q(r)$ in terms of $p_F(r)$ and $p_B(r)$, denoting, respectively, the forward and backward probabilities with the imposed analytical form [e.g., $p(r) \propto r^{-\mu}$]:

$$q(r) = p_F(r) + p_B(r) - p_F(r)\, p_B(r) \tag{1}$$

with

$$p_F(r) = p(r) \prod_{l=r+1}^{r_{max}} [1 - \kappa_2\, p_F(l)] \tag{2}$$

and

$$p_B(r) = p(r) \left\{ \prod_{l=1}^{r_{max}} [1 - \kappa_2\, p_F(l)] \right\} \prod_{l=1}^{2r-1} [1 - \kappa_2\, p_B(l)] \tag{3}$$

where r_{max} is the cutoff distance in the distribution $p(r)$,[3] and $\kappa_2 = f(1-f)$, with f the particle density per channel.[3] Besides the fact that here interaction distances are distributed over an interaction range, an important difference from the fixed-distance model[1,2] is that in the present case, each particle belongs to many pairs of possible interactions. Note also that for similar reasons, there is a bias in the effective distribution toward large interaction distances. Indeed when drawing a low value of r from $p(r)$ in the sequential procedure, there is a greater chance that the second particle of the pair is already involved in a previous pairing. As a result the effective probability for long-distance interactions is larger than predicted by the preset distribution $p(r)$.

The issue now arises of defining a quantity which can be identified as an interaction potential in a discrete lattice gas. We propose the following heuristic argument. We evaluate the rate of momentum exchange caused by the nonlocal interaction

$$F(r) = \gamma \kappa_2^2 q(r) \tag{4}$$

[3] Note that if desired operationally, Eqs. (1)–(3) can be inverted numerically to obtain a function $p(r)$ such that the effective distribution $q(r)$ is of given analytical form.

where γ is a numerical factor whose value corresponds to the average amount of momentum transfer ($\gamma = 4/3$ and $\gamma = 1$ for the models shown in Figs. 1a and 1b, respectively). Interpreting $F(r)$ in (4) as a force, we define the "pair potential" as the discrete analog of the potential in continuum mechanics:

$$\begin{aligned} u(r) &= -\kappa_2^{-2} \sum_{l=1}^{r} F(l) \\ &= -\sum_{l} \gamma q(l) \\ &= -\gamma \mathscr{F}(r) \end{aligned} \tag{5}$$

where $\mathscr{F}(r)$ is the repartition function corresponding to the distribution $q(r)$. Then using Eqs. (1)–(3), we see that $u(r)$ is well defined once $p(r)$ is fixed. For instance, if we use the power-law distribution $p(r) \propto r^{-\mu}$ such that the interactions are repulsive for $r = 1$ and attractive for $r = 2, \ldots, r_{\max}$, then $u(r)$ exhibits a form compatible with the expected typical pair interaction potential, as shown in Fig. 2.

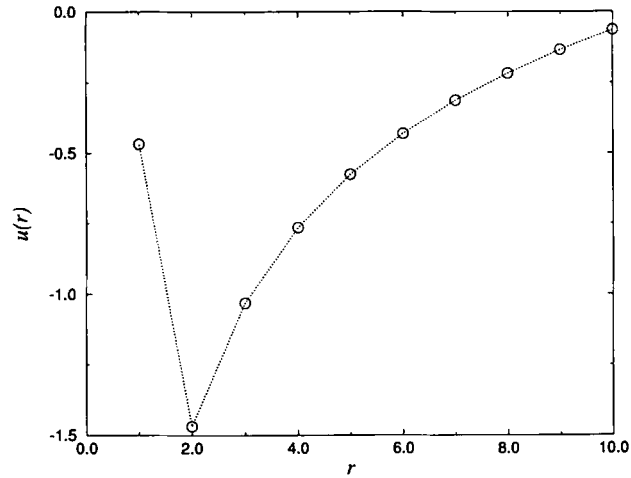

Fig. 2. Pair interaction potential: $u(r)$ for a power-law distribution $p(r) \propto r^{-\mu}$ for $1 \leqslant r \leqslant r_{\max}$, with $\mu = 1.2$ and $r_{\max} = 10$. Potential units are arbitrary.

3. DENSITY FLUCTUATION CORRELATIONS

The next issue is the influence of the nonlocal interactions on the density fluctuation correlations in the lattice gas, which is most conveniently measured by the static structure factor[5] defined by

$$\rho S(k) = \frac{1}{T} \sum_{t=1}^{T} \sum_{i,j} \delta n_i^*(k, t)\, \delta n_j(k, t) \tag{6}$$

where ρ is the density per node, and

$$\delta n_i(k, t) = \sum_{\mathbf{x}} e^{-i\mathbf{k}\cdot\mathbf{x}} [n(\mathbf{x}, \mathbf{c}_i; t) - f] \tag{7}$$

is the fluctuation of the channel occupation numbers n_i ($i = 0,..., b$). In the ideal lattice gas (whose dynamics is governed by propagation-collision rules) there are no static density correlations and the static structure factor is a constant[5]:

$$S^0(k) = (1 - f)(1 - \delta(k)) \tag{8}$$

By analogy with the statistical mechanical theory of continuous fluids,[6] we write

$$\frac{S(k)}{S^0(k)} = 1 + fh(k) \tag{9}$$

where $h(k)$ is the Fourier transform of the pair correlation function $[g(r) - 1]$ and is therefore related to the potential of mean force $\phi(r)$ since $g(r) = \exp[-\beta\phi(r)]$ (here β is an arbitrary constant). So by measuring the density fluctuation correlations in lattice gas simulations, we can extract a function $\phi(r)$ from the measured static structure factor. The results are shown in Fig. 3: both the radial distribution function $g(r)$ and the potential function $\phi(r)$ are reminiscent of those obtained in real fluid measurements.[7] The connection between the potential of mean force $\phi(r)$ and the interaction potential $u(r)$ discussed in Section 2 remains to be clarified.

Another interesting feature is worth mentioning. Consider the LGA is in the appropriate density range for spinodal decomposition (see Section 4). Then one could effectively "quench" the system by increasing the interaction range. By measuring $S(k)$ at successively increasing values of $r_{\max}$ we find that $S(k)$ increases dramatically at low k. Following the lines of heuristic reasoning and anticipating a result of Section 4, we infer that

$$S(k \to 0) \simeq \frac{1 - f}{1 - \gamma\kappa_3 \langle r \rangle_q} \tag{10}$$

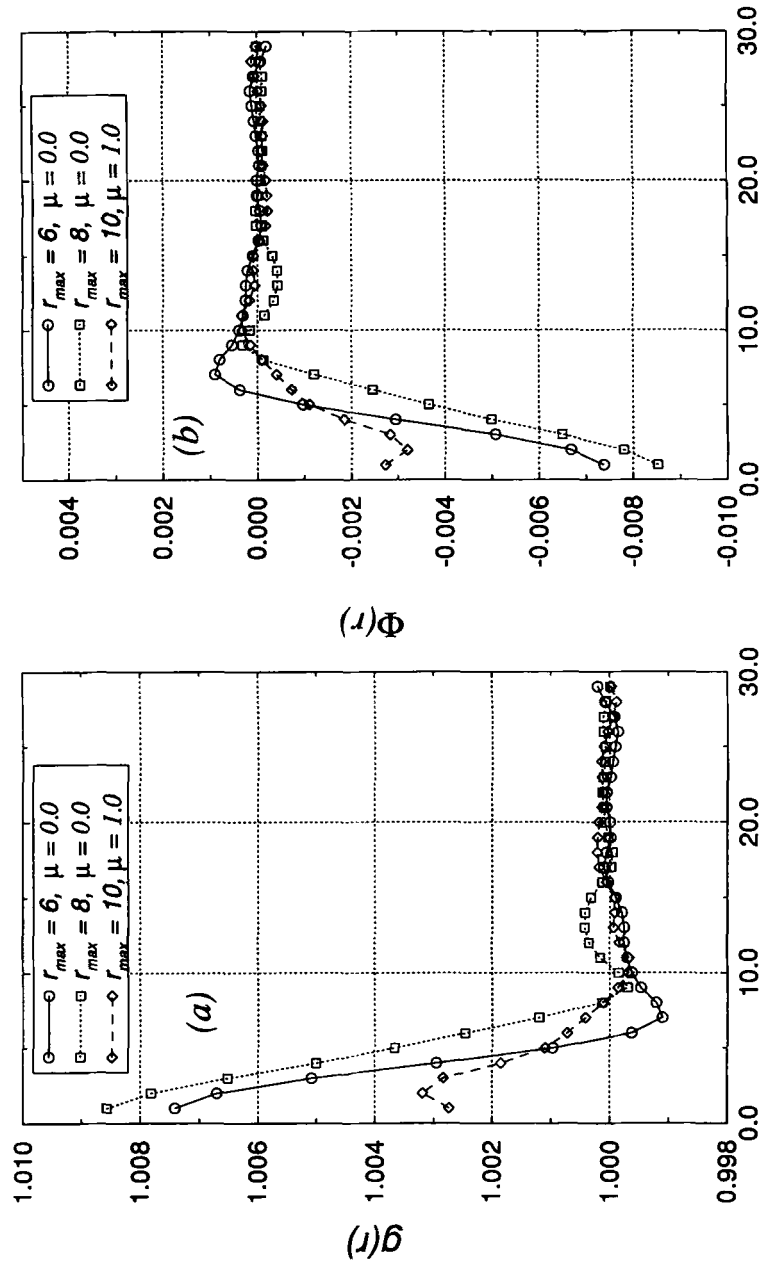

Fig. 3. (a) Radial distribution function $g(r)$. (b) Potential function $\Phi(r) \equiv \ln(g(r))$. Probability distribution $p(r) \propto r^{-\mu}$ for $1 \leqslant r \leqslant r_{\max}$; $r_{\max} = 6$, $\mu = 0$ (circles), $r_{\max} = 8$, $\mu = 0$ (squares), $r_{\max} = 10$, $\mu = 1$ (diamonds). Lines are guides to the eye. Mean channel density $f = 0.1$; lattice size 512×512; $g(r)$ measured over 500 time steps.

where the denominator follows from the expression for the compressibility (see Section 4). Here $\langle r \rangle_q$ is the expectation of r computed with the distribution $q(r)$. Since $\langle r \rangle_q$ increases with $r_{\max}$, $S(k \to 0)$ grows accordingly as expected when the phase transition is approached. Further analysis will be presented in a forthcoming paper.

4. EQUILIBRIUM PROPERTIES

The pressure at global equilibrium is given by[8]

$$p = \frac{1}{2V} \sum_{\mathbf{x} \in \mathscr{L}} \sum_i \langle n_i(\mathbf{x}) + m_i(\mathbf{x}) \rangle \tag{11}$$

where V is the number of nodes of the automaton universe, $\sum_{\mathbf{x} \in \mathscr{L}} \sum_i \langle n_i(\mathbf{x}) \rangle$ is the momentum transport due to propagation, and $\sum_{\mathbf{x} \in \mathscr{L}} \sum_i \langle m_i(\mathbf{x}) \rangle$ is the momentum flux due to NLIs. Then the hydrostatic pressure can be evaluated as follows:

- The convective momentum flux is the total momentum carried by moving particles in the fluid. On each node in the FHP-III model, there are six channels with velocity 1 and one zero-velocity channel, so that

$$\sum_{\mathbf{x} \in \mathscr{L}} \sum_i \langle n_i(\mathbf{x}) \rangle = V \tfrac{6}{7} \rho \tag{12}$$

  where ρ is the average density per node.

- The nonlocal momentum flux is caused by NLIs. The value of this flux is clearly given by

$$\sum_{\mathbf{x} \in \mathscr{L}} \sum_i \langle m_i(\mathbf{x}) \rangle = 3V\gamma\kappa_2^2 \sum_r rq(r) \tag{13}$$

  since on the average each NLI causes a momentum flux of value γr and on a given node three particles may independently be involved in an interaction.

Consequently

$$p = 3f - \tfrac{3}{2}\gamma\kappa_2^2 \langle r \rangle_q \tag{14}$$

with $f = \rho/7$ and $\langle r \rangle_q = \sum_r rq(r)$. The first term on the r.h.s. of (14) is the kinetic pressure of the ideal lattice gas and the second term as given in this mean-field evaluation depends only on the first moment of the distance

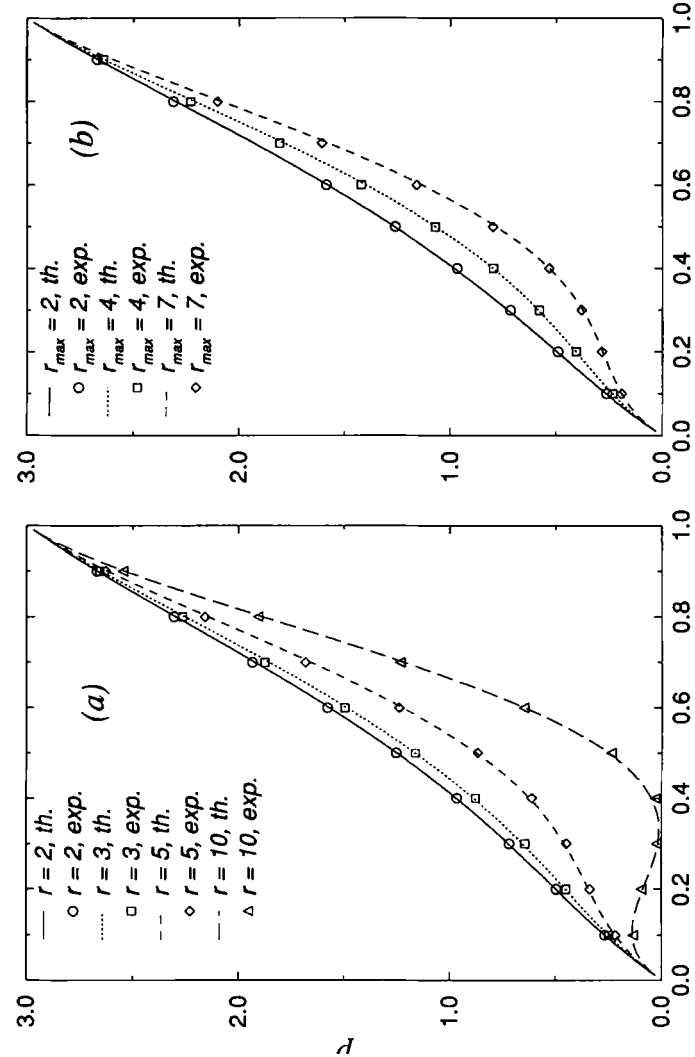

Fig. 4. Pressure versus density. (a) Fixed-distance interactions; (b) distributed-distance interactions, with "flat" distribution $p(r) \propto r_{max}^{-1}$. Symbols are experimental data, curves are theoretical predictions. Fixed distances r and cutoff distances r_{max} are as indicated. Lattice size 512×512; each point is obtained by averaging over 300 time steps.

distribution $q(r)$. Note that for fixed-distance interaction models, $q(r)=\delta(r-l)$ and (14) becomes for the model of Fig. 1a (with $\gamma=4/3$)

$$p=3f-2l\kappa_2^2 \tag{15}$$

as given in refs. 1 and 2.

From (14) it follows that the compressibility is given by

$$\begin{aligned}\chi&=\frac{1}{\rho}\frac{\partial\rho}{\partial p}\\&=\frac{1}{\frac{3}{7}\rho(1-\gamma\langle r\rangle_q\kappa_3)}\\&=\frac{\chi^0}{1-\gamma\langle r\rangle_q\kappa_3}\end{aligned} \tag{16}$$

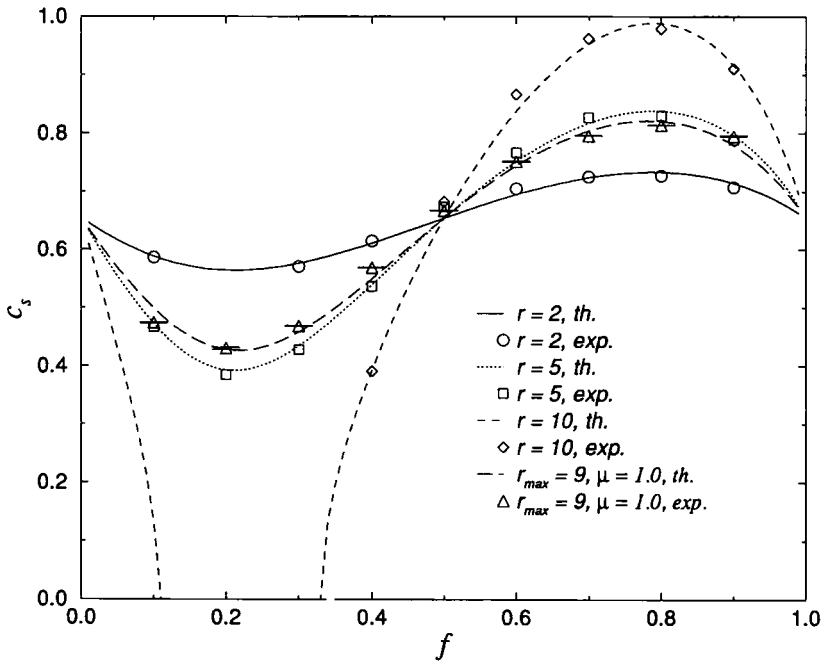

Fig. 5. Sound velocity versus density. Circles, squares, diamonds (resp. full, dotted, and dashed lines) correspond to fixed-distance interactions; triangles (long-dashed line) correspond to "flat" distributed-distance interactions. Symbols are experimental data, curves are theoretical predictions. Fixed distances r and cutoff distances r_{max} are as indicated. Lattice size 512×512; each point is obtained by averaging over ten runs of 2500 time steps.

where $\kappa_3 \equiv f(1-f)(1-2f)$ and χ^0 is the compressibility of the ideal gas. By using $S(k \to 0) = \rho\beta^{-1}\chi_{\text{th}}$,[6] and the *thermodynamic* pressure of the ideal gas $p_{\text{th}} = -b\beta^{-1}\ln(1-f)$, which yields the compressibility $\chi^0_{\text{th}} = \rho^{-1}\beta(1-f)$ (with $\beta^{-1} = c_0^2 = 3/7$ for the FHP-III model), we obtain Eq. (10).

The compressibility equations (14) yields the square of the sound velocity c_s

$$c_s^2 = \frac{\partial p}{\partial \rho} = c_0^2[1 - \gamma\kappa_3\langle r\rangle_q] \tag{17}$$

Equation (17) is valid as long as $\partial p/\partial\rho > 0$; when $\partial p/\partial\rho < 0$, the density fluctuations show an explosive behavior and the system separates into two phases (i.e. for $\langle r\rangle_q > 7.79$). In Fig. 4 we show the results of measurements of the pressure as given by Eq. (11), compared to the theoretical prediction (14); in Fig. 5, the theoretical sound velocity (17) is compared to the simulation results (for the experimental method, see e.g., ref. 2). Experimental evidence of spinodal decomposition is given in Fig. 6, where the evolution of the density distribution shows how phase separation takes place in the automaton.

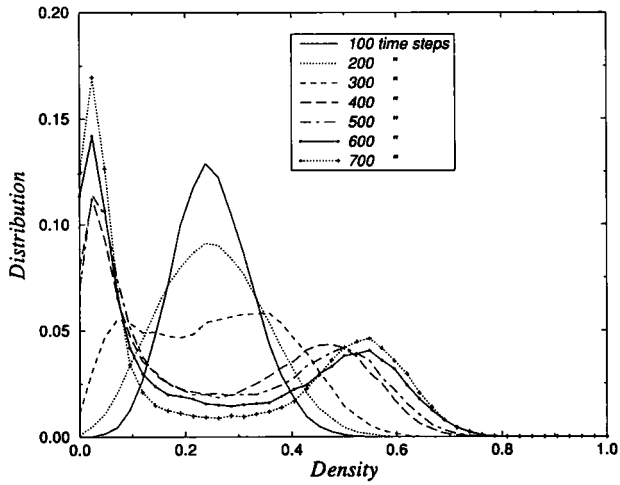

Fig. 6. Evolution of the density distribution, measured every 100 time steps for a total duration of 700 time steps. The evolution shows horizontal separation of density peaks characteristic of spinodal decomposition, as opposed to vertical growth of peaks in nucleation and growth processes. Lattice size 512×512; $\mu = 0$; $r_{\max} = 20$; density values are coarse grained by averaging over each node and its six nearest neighbors.

5. TRANSPORT COEFFICIENTS

5.1. Microdynamical and Lattice Boltzmann Equations

The evolution of the automaton is obtained by applying successively the nonlocal interaction routine, the collision routine, and the propagation routine. This computational procedure is the operational realization of the microscopic dynamics of the automaton whose mathematical formulation is given by the microdynamical equation

$$n(\mathbf{x}+\mathbf{c}_i, \mathbf{c}_i; t+1) = \mathscr{C}_i\{\mathscr{I}[n(\mathbf{x}; t)]\} \tag{18}$$

where $n(\mathbf{x}, \mathbf{c}_i; t)$ is the Boolean occupation variable of channel i at node $\mathbf{x}$ at time t. Here $\mathscr{C}$ and $\mathscr{I}$ are the local collision and nonlocal interaction operators, respectively. The explicit expression of the nonlocal operator $\mathscr{I}$ reads

$$\mathscr{I}_i = \tfrac{1}{3}\sum_r q(r) \sum_{j=-1}^{+1} \mathscr{I}^r_{i,\,i+j} \tag{19}$$

with (for the model of Fig. 1a)[4]

$$\begin{aligned}
\mathscr{I}^r_{i,\,i} n(\mathbf{x}; t) &= [\bar{n}_i(\mathbf{x}; t)\, n_{i+3}(\mathbf{x}; t)][n_i(\mathbf{x}+r\mathbf{c}_i; t)\, \bar{n}_{i+3}(\mathbf{x}+r\mathbf{c}_i; t)] \\
&\quad - [n_i(\mathbf{x}; t)\, \bar{n}_{i+3}(\mathbf{x}; t)][\bar{n}_i(\mathbf{x}-r\mathbf{c}_i; t)\, n_{i+3}(\mathbf{x}-r\mathbf{c}_i; t)] \\
\mathscr{I}^r_{i,\,i\pm1} n(\mathbf{x}; t) &= [\bar{n}_i(\mathbf{x}; t)\, n_{i\mp1}(\mathbf{x}; t)][n_i(\mathbf{x}+r\mathbf{c}_{i\pm1}; t)\, \bar{n}_{i\mp1}(\mathbf{x}+r\mathbf{c}_{i\pm1}; t)] \\
&\quad - [n_i(\mathbf{x}; t)\, \bar{n}_{i\mp1}(\mathbf{x}; t)][\bar{n}_i(\mathbf{x}-r\mathbf{c}_{i\pm1})\, n_{i\mp1}(\mathbf{x}-r\mathbf{c}_{i\pm1}; t)]
\end{aligned} \tag{20}$$

where $\bar{n} \equiv 1 - n$.

Taking the average of Eq. (18) over a nonequilibrium ensemble, and making the *molecular chaos* assumption, one obtains the lattice Boltzmann equation

$$f(\mathbf{x}+\mathbf{c}_i, \mathbf{c}_i; t+1) = \mathscr{C}_i\{\mathscr{I}[f(\mathbf{x}; t)]\} \tag{21}$$

where $f(\mathbf{x}, \mathbf{c}_i; t) \equiv \langle n(\mathbf{x}, \mathbf{c}_i; t)\rangle$ is the singlet distribution function of channel i at node $\mathbf{x}$ at time t. In this equation, the operators $\mathscr{C}$ and $\mathscr{I}$ act on the distribution function f (not on the Boolean variables n_i).

[4] Channel indices are numbered counterclockwise from 0 to 5 for moving particles and 6 for the rest particle, and indices i and $i+j$ are taken modulo 6.

5.2. Linearized Lattice Boltzmann Equation

Considering small deviations from local equilibrium

$$f(\mathbf{x}, \mathbf{c}_i; t) = f + \delta f(\mathbf{x}, \mathbf{c}_i; t) \tag{22}$$

we can linearize the lattice Boltzmann equation (21) for the perturbation δf. Denoting by $\boldsymbol{\Omega}$ the usual linearized collision operator and by $\boldsymbol{\Lambda}$ the linearized NLI operator,

$$\delta f'(\mathbf{x}, \mathbf{c}_i; t) = (\mathbf{1} + \boldsymbol{\Lambda})_{ij}\, \delta f(\mathbf{x}, \mathbf{c}; t) \tag{23}$$

we find for the linearized lattice Boltzmann equation

$$\delta f(\mathbf{x} + \mathbf{c}_i; \mathbf{c}_i; t+1) = (\mathbf{1} + \boldsymbol{\Omega})_{ij}\, (\mathbf{1} + \boldsymbol{\Lambda})_{jk}\, \delta f(\mathbf{x}, \mathbf{c}_k; t) \tag{24}$$

We develop the perturbations δf in Fourier modes

$$\delta f(\mathbf{x}, \mathbf{c}_i; t) = \sum_{\mu} \sum_{\mathbf{k}} \psi_{\mu}(\mathbf{k}, \mathbf{c}_i)\, e^{i\mathbf{k}\cdot\mathbf{x} + z_{\mu}(\mathbf{k})t} \tag{25}$$

and rewrite Eq. (24) in Fourier space to obtain the eigenvalue equation for the automaton

$$[e^{z_{\mu}(\mathbf{k}) + i\mathbf{k}\cdot\mathbf{c}} - (\mathbf{1} + \boldsymbol{\Omega})(\mathbf{1} + \boldsymbol{\Lambda})]_{ij} \mid \psi_{\mu}(\mathbf{k}, \mathbf{c}_j)\rangle = 0 \tag{26}$$

This equation is formally identical to the eigenvalue equation for the fixed-distance model,[2] but the operator $\boldsymbol{\Lambda}$ is now a linear combination of the corresponding fixed-distance operators. The three slow (hydrodynamic) modes of interest are the shear mode, denoted ψ_{ν}, whose eigenvalue corresponds to the kinematic viscosity ν, and the two sound modes $\psi_{\sigma=\pm}$ related to the sound velocity c_s and damping coefficient Γ.

5.3. Transport Coefficients

As mentioned, the operator $\boldsymbol{\Lambda}$ is a linear combination of fixed-distance NLI operators

$$\boldsymbol{\Lambda}_{ij} = \sum_{r} q(r)\, \boldsymbol{\Lambda}_{ij}^{*r} \tag{27}$$

where $\boldsymbol{\Lambda}_{ij}^{*r}$ denotes the NLI operators at distance r. So the results for the fixed-distance interaction operators can be extended to the present model (see ref. 2 for details). The main difference is that the distance r is now replaced by its mean value $\langle r \rangle_q$, and r^2 by the variance $\langle r^2 \rangle_q = \sum_r r^2 q(r)$. Expanding the eigenvalues in powers of k,

$$z_{\mu}(\mathbf{k}) = (\imath k)\, z_{\mu}^{(1)} + (\imath k)^2\, z_{\mu}^{(2)} + \cdots \tag{28}$$

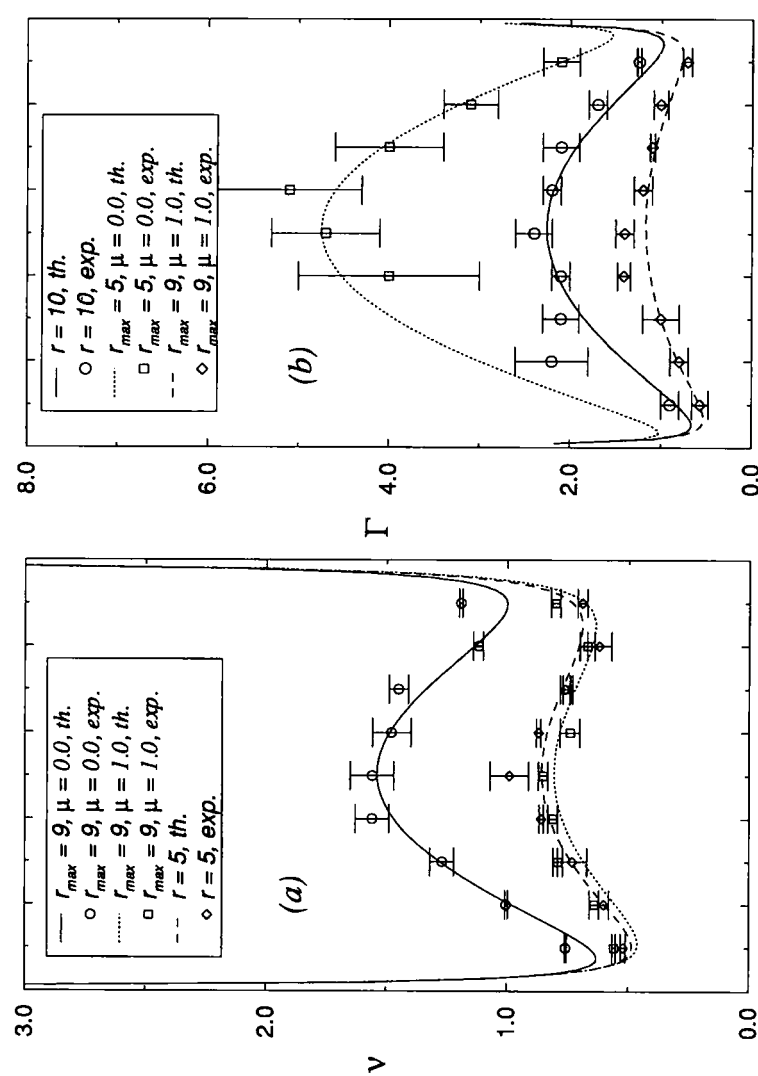

Fig. 7. (a) Kinematic viscosity ν versus density; (b) sound damping coefficient Γ versus density. Symbols are experimental data, curves are theoretical predictions, conditions are as indicated. Lattice size 512×512; each point is obtained by averaging over 100 runs of 2500 time steps.

we obtain

$$\begin{aligned} z_\sigma^{(1)} &= \pm c_s, & z_\nu^{(1)} &= 0 \\ z_\sigma^{(2)} &= \Gamma = \tfrac{1}{2}(\nu + \zeta), & z_\nu^{(2)} &= \nu \end{aligned} \tag{29}$$

with

$$\begin{aligned} \nu &= \nu_0(1 - \tfrac{1}{3}\langle r\rangle_q\kappa_3)(1 - \langle r\rangle_q\kappa_3) + \tfrac{1}{12}\langle r\rangle_q\kappa_3(1 - \tfrac{1}{2}\langle r\rangle_q\kappa_3) + \tfrac{1}{8}\langle r^2\rangle_q\kappa_2 \\ \zeta &= \zeta_0(1 - \tfrac{4}{3}\langle r\rangle_q\kappa_3) - \tfrac{1}{21}\langle r\rangle_q\kappa_3 + \tfrac{1}{4}\langle r^2\rangle_q\kappa_2 \end{aligned} \tag{30}$$

ν_0 and ζ_0 are the kinematic and bulk viscosities of the standard FHP-III model,

$$\begin{aligned} \nu_0 &= \frac{1}{14}\left(\frac{1}{\omega_\nu} - \frac{1}{2}\right) \\ \zeta_0 &= \frac{1}{14}\left(\frac{1}{\omega_\zeta} - \frac{1}{2}\right) \end{aligned} \tag{1}$$

with

$$\begin{aligned} \omega_\nu &= \kappa_2(7 - 8\kappa_2) \\ \omega_\zeta &= 7\kappa_2(1 - 2\kappa_2) \end{aligned} \tag{32}$$

Excellent agreement is obtained between the simulation data and the theoretical results, as shown in Fig. 7.

6. COMMENTS

The question was raised by Gerits *et al.*[2] that models with nonlocal fixed interaction distance lack detailed balance and that therefore their equilibrium distribution is not known. In fact, with a proper redefinition of the configuration space, it can be shown that a generalized semi-detailed balance holds for LGAs with NLIs and that an H-theorem exists. The mean-field theory is found to correctly predict macroscopic equilibrium and transport properties. Fluctuation correlations were measured and the static structure factor was used to extract the LGA analog of a potential of mean force. The statistical mechanical theory will be discussed in a forthcoming paper.

APPENDIX. EVALUATION OF $q(r)$

Here we show how to compute the effective automaton distance distribution $q(r)$ from a given probability distribution $p(r)$. The algorithmic procedure considers each node sequentially. Define the node currently examined as the "center node" A and define the "forward node" F and "backward node" B located along the direction of interaction at a distance r on each side of A. Now each particle on A may interact with at most one particle located *either* on F *or* on B. However, since the algorithm is sequential, the forward and backward probabilities are different: a backward interaction is possible only if the particle on A has not interacted before, while a forward interaction is independent of previous interactions involving node A.

• *Forward interaction probability* $p_F(r)$. Suppose that configurations on A and F are favorable (see Fig. 1). Then the only additional condition is that the particle on F cannot have been involved previously in an interaction from a distance larger than r. This "nonevent" has the probability

$$\prod_{l=r+1}^{r_{\max}} [1-\kappa_2 p_F(l)] \tag{A1}$$

Consequently, the equation for p_F is given by

$$p_F(r) = p(r) \prod_{l=r+1}^{r_{\max}} [1-\kappa_2 p_F(l)] \tag{A2}$$

• *Backward interaction probability* $p_B(r)$. We must consider that (i) the particle on A has not been involved in a previous (forward) interaction, (ii) the particle on B has not been paired successfully with another particle when B was a center node (forward interaction), and (iii) the particle on B has not been paired successfully with a center node located between B and A (backward interaction). The corresponding probabilities are as follows.

(i) No interaction with A as a foward node:

$$\prod_{l=1}^{r_{\max}} [1-\kappa_2 p_F(l)] \tag{A3}$$

(ii) No interaction with B as a center node: same as (A3).

(iii) No interaction with B as backward node:

$$\prod_{l=1}^{r-1} [1-\kappa_2 p_B(l)] \tag{A4}$$

The backward probability is therefore

$$p_B(r) = p(r) \left\{ \prod_{l=1}^{r_{\max}} [1 - \kappa_2 p_F(l)] \right\} \prod_{l=1}^{2r-1} [1 - \kappa_2 p_B(l)] \tag{A5}$$

As a result, $q(r)$ is expressed as a combination of p_B and p_F, given that forward and backward interactions are mutually exclusive:

$$q(r) = p_F(r) + p_B(r)[1 - p_F(r)] \tag{A6}$$

In the case of fixed-distance interactions (at a distance l_0), the above considerations do not apply and the distribution reduces to

$$q(r) = \delta_{r, l_0} \tag{A7}$$

ACKNOWLEDGMENTS

O.T. has benefited from a grant from the Institut pour l'Encouragement de la Recherche Scientifique dans l'Industrie et l'Agriculture (IRSIA, Belgium). J.P.B. acknowledges support from the Fonds National de la Recherche Scientifique (FNRS, Belgium).

REFERENCES

1. C. Appert and S. Zaleski, Lattice gas with a liquid–gas transition, *Phys. Rev. Lett.* **64**:116 (1990); Dynamical liquid–gas phase transition, *J. Phys. II France* **3**:309 (1993).
2. M. Gerits, M. H. Ernst, and D. Frenkel, Lattice gas automata with attractive and repulsive interactions, *Phys. Rev. E* **48**:988 (1993).
3. O. Tribel and J. P. Boon, Lévy laws for lattice gas automata, in *Pattern Formation and Lattice Gas Automata* (Fields Institute of Mathematics, Waterloo, 1995).
4. D. d'Humières and P. Lallemand, Numerical simulations of hydrodynamics with lattice gas automata in two dimensions, *Complex Systems* **1**:599 (1987).
5. P. Grosfils, J. P. Boon, R. Brito, and M. H. Ernst, Statistical hydrodynamics of lattice gas automata, *Phys. Rev. E* **48**:2655 (1993).
6. J. P. Boon and S. Yip, *Molecular Hydrodynamics* (Dover, New York, 1991), Chapter 2.
7. P. Egelstaff, *An Introduction to the Liquid State* (Academic Press, London, 1967).
8. R. Feynman, *The Feynman Lectures on Physics* (Addison-Wesley, Reading, Massa chusetts, 1964), Vol. 2.
9. M. J. Ernst and H. J. Bussemaker, *J. Stat. Phys.*, this issue.
10. J. R. Dorfman, T. R. Kirkpatrick, and J. V. Sengers, *Annu. Rev. Phys. Chem.* **45**:213 (1994).